Aygun, H. McCann. F. 2020. Structural and acoustical performance of recycled glass bead panels. *Construction & Building Materials*. 258, 119581.

Structural and acoustical performance of recycled glass bead panels

Haydar Aygun[1] and Finian McCann[2*]

School of the Built Environment and Architecture, London South Bank University, 103 Borough Road, London, UK

[1] aygunh@lsbu.ac.uk; [2] mccannf@lsbu.ac.uk; * corresponding author

Abstract

An investigation is conducted to determine the structural and acoustical properties of panels comprising a core of recycled glass beads bound in a matrix of polyurethane resin enveloped by two fibreglass facing sheets. This investigation is conducted in order assess the suitability of recycled glass bead panels in multifunctional applications in the built environment, especially in urban, built-up or noisy environments where both structural resistance and acoustic insulation are beneficial. In order to assess the acoustical performance of the panels, experiments to determine the transmission loss and absorption coefficients are performed using the transfer function method. It is shown that the panels provide effective insulation for typical urban built environments. Experiments are also described that are conducted to determine the modulus of elasticity of the fibreglass sheets, the compressive strength of the bead cores and the behaviour of the recycled glass bead panels when loaded in bending. A design method to predict the ultimate moment resistance of a panel in bending is proposed, which is shown to provide conservative and safe-sided predictions when compared to the experimental results. It is shown that, when employed in a flooring system, recycled glass bead panels can achieve usable spans under typical floor loads expected in commercial and residential structural applications, while also possessing the acoustic insulation performance required of a modern and comfortable dwelling or workspace. This combination of structural and acoustic performance has considerable potential to increase material efficiency in construction.

1. Introduction

The design of effective acoustic insulation in buildings and noise barriers is important to ensure that the ever-expanding residential and commercial infrastructure associated with increasing development, industry and population do not impact negatively on the normal everyday use of the built environment. In addition, there is an increased need to produce practical designs that also incorporate benefits to the environment and to reduce the impact on the well-being of building occupants [1,2]. Meeting the combined demands of increasing population density and limited resource availability has become a key challenge facing the structural and infrastructural designers of this century.

It has been advised [3] that, in order to meet current demand for housing stock in the United Kingdom, 260,000 new residential units are required to be constructed each year until 2023. Meeting this demand within such a short period of time could be achieved by developing faster methods of construction, in addition to developing additional sites suitable for construction. Modular and offsite construction methods, whereby structural units or modules are fabricated offsite and then assembled onsite, are becoming increasingly popular in the construction industry owing to their potential to reduce construction time [4], reduce overall costs of manufacture [4] and increase safety and reliability during construction and operation [5]; thus, increased research and development has focussed on the use of various construction materials and fabrication techniques in offsite construction, which have been summarised in a number of review studies [6–10]. The need to develop residential sites within urban centres is

continuously increasing due to rising global urbanisation. With construction space already at a premium within most urban centres, the need to construct residential units in noisy or vibration-prone environments such as in proximity to highways and rail corridors is increasing [11,12]. When considering these particular challenges that are facing the construction industry, structural solutions that can combine speed and reliability of construction with the ability to provide a built environment free from excessive noise or uncomfortable vibrations offer considerable advantages to structural designers.

Recycled glass bead panels (RGBPs) are structural components comprising two fibreglass facing sheets surrounding an inner core of recycled glass beads bonded in a matrix of polyurethane (PU) resin, as shown in Figure 1. The inclusion of recycled glass beads in construction materials has a number of precedents, including in concrete and cement mortar [13,14], in asphalt [15] and in masonry [16]. This previous research has demonstrated that the structural performance of materials containing glass beads is at least as effective as that of conventional analogues. However, although recycled glass bead panels are available commercially [17] and the mechanical behaviour of structural glass is relatively well understood with data available for properties such as tensile strength, compressive strength and modulus of elasticity [18], there is limited literature [19] concerning the behaviour of polyurethane-bound recycled glass bead core as a load-transferring mechanism in itself. The present study aims to expand upon existing test results for the acoustical behaviour and compressive resistance of the material and discuss the results of bend tests conducted on full-scale panel specimens.

The low weight and portability of RGBPs make them ideally suited to applications in modular construction, where whole units can be fabricated offsite and transported to their final location. Alternatively, the panels can be easily manipulated onsite, making them also well-suited for temporary applications such as emergency shelters or as temporary noise barriers. At present, there is a limited number of manufacturers of such panels, and little to no focussed research on the potential for their optimisation. The particulate nature of the cores creates a large number of air voids within them, which reduces vibrations [20] and lowers the thermal conductivity of the panels. This latter characteristic ensures an enhanced thermal insulating performance, leading to a high degree of thermal energy efficiency during the operational life-span of a building structure. When considering that they are also fabricated predominantly from recycled materials, the environmental sustainability of structures incorporating RGBPs is considerably enhanced [21]; in addition, the resilience and durability of glass [18] and polyurethane [22,23] materials against environmental effects is well-attested. Since glass is inherently non-combustible, the overall fire resistance of the panels can be enhanced through optimisation of the organic polymer content. When considering these factors together, recycled glass bead panels thus represent a multifunctional structural solution that can be used as a floor panel, wall panel, cladding panel, roofing element or indeed as a dedicated noise barrier, with advantages including reduced weight, increased portability, increased thermal energy efficiency, increased acoustic insulation, increased fire resistance and long-term resilience against environmental effects.

The panels investigated in the present study are fabricated on an industrial scale by initially coating beads formed from crushed recycled glass in a PU resin in order to bind the core together; PU is preferred over other polymers since it is easily prepared onsite and, after combination of its constituent components, is liquid at room temperature without the need for pre-heating (as would polypropylene). For larger mixes, the PU curing time can be controlled via material selection. While also dependent on the glass bead diameter, the strength of the core is mainly controlled through specification of the resin-to-bead ratio; the samples examined in the present study contained 7% by volume (the typical range for the ratio is 6 – 8%). After

mixing, the resultant core is then formed to the required thickness and slab breadth and passed through an extruder. An epoxy adhesive is applied to two fibreglass facing sheets which are then pressed mechanically onto the core. Finally, the panels are cut to size and allowed to settle. Given that the manufacturing process is not overly complicated and that the main constituent material, i.e., recycled glass, is relatively inexpensive to source, RGBPs thus offer a cost-effective and environmentally-sustainable solution to meet the increasing demands of urban development. The main parameters governing the acoustical and structural properties of the bead core are the nominal bead diameter range, porosity, density and the relative amount of PU binder.

Previous studies on the impact of noise from highway networks found that the frequency spectrum of A-weighted road traffic noise is typically between 125 Hz and 4000 Hz [24]. For applications as highway noise barriers, good performance in the mid frequency range between 500 Hz and 1500 Hz is essential in order to ensure efficacy against road traffic noise [2]. The effectiveness of a noise barrier is related to the characteristics of their constituent materials, particularly the absorption coefficient of the material and the surface impedance [25]. There are other characteristics that lend towards the overall effectiveness of a material as an acoustic absorber such as characteristic impedance, porosity, density, flow resistivity and tortuosity. Conventional highway noise barriers are formed from a range of materials, including masonry, earthwork, porous materials such as polymer foams, and fibrous materials such as mineral wool [25]. Porous materials, such as the glass bead mixes under investigation in the present study, are particularly well-suited to absorb sound, leading to a lower sound levels being reflected and transmitted [26,27]. The flow resistivity and insertion loss generally increase as the density of the material increases. Fibrous materials are often used in noise barriers because of their characteristic anisotropic and cellular structure [28]. This anisotropy, which is due to the orientation of the fibres, means that the subsequent flow resistivity is direction-dependent: it is lower along the panel in a planar direction, while at a normal incidence, the flow resistivity increases. The effectiveness of a simple noise barrier is typically limited to a reduction of sound approximately 15 dB due to diffraction, and barriers are most efficient at mitigating middle and high frequencies [29]. The noise contribution from road traffic vehicles differs dependent on the type, size, weight and speed of the vehicle, effects of the road surface materials and meteorological effects such as temperature, humidity and wind direction [30–32]. As the acoustic properties of traffic noise reducing devices such as highway noise barriers is frequency dependent, there is a need to define a generic noise spectrum for test purposes [33]. In terms of controlling noise in a building structure, any solid structure may be used as a noise barrier between the sound source and the receptor point as long as the barrier has a sound transmission loss of at least 10 dB greater than the desired noise reduction, in accordance with typical noise pollution limits [11].

In summary, the aim of the present study is to determine the acoustical and structural properties of recycled glass bead panels in order to assess their suitability for civil engineering applications, especially in noisy urban environments, either as structural panel components that also offer acoustic insulation or as dedicated noise barriers. A method is described to determine the sound absorption coefficient and transmission loss of the panels from data obtained using the transfer function method in a bespoke impedance tube system, with the results of such experiments on three samples discussed. Structural and mechanical tests are then described in order to determine the modes of failure, the ultimate resistances, the initial linear stiffness and the ductility of the recycled glass bead panels. A simple design equation for the cross-sectional moment resistance of the panels is proposed and compared against the experimental results, with safe-sided predictions observed.

2. Acoustical experiments

In this section, experiments [19] conducted on RGBP specimens to measure acoustic reflection, sound absorption and sound transmission loss are described. The impedance tube method, which is performed via the transfer function method in accordance with BS EN ISO 10543-2:2001 [33], was employed to determine the acoustic properties. It should be noted that while the use of an impedance tube is useful at a developmental stage, testing of full-scale specimens must be conducted in order to achieve a final characterisation of the system, especially when considering how the joints between the panels can affect the acoustic response.

Three cylindrical specimens cut from full RGBPs, as shown in Figure 2, were tested: Specimens C01-4-150 and C02-1-150 were 130 mm thick with a nominal glass bead diameter of 4–8 mm and 1–2 mm, respectively, while specimen C03-1-050 was 50 mm thick with a nominal glass bead diameter of 1–2 mm. The density of the 1–2 mm diameter bead mixes was 395 kg/m^3 on average, while that of the 4–8 mm diameter bead mixes was 440 kg/m^3 on average.

2.1 Transfer function theory

The experimental procedure is based on the acoustic reflection coefficient at normal incidence being determined from the measured transfer function between two microphone positions in front of the tested material. The sound pressures of the incident wave p_i and the reflected wave p_r are respectively [34]:

$$p_i = p^+ e^{ikx} \tag{1}$$

and

$$p_r = p^- e^{-ikx} \tag{2}$$

where $p^+$and p^- are the magnitudes of the incident and reflected waves respectively, and *k* is the complex propagation constant.

The sound pressure p_1 and p_2 at the two microphone positions are:

$$p_1 = p^+ e^{ikx_1} + p^- e^{-ikx_1} \tag{3}$$
$$p_2 = p^+ e^{ikx_2} + p^- e^{-ikx_2} \tag{4}$$

Where x_1 is the distance between the sample and the centre of the further microphone, and x_2 is the distance between the sample and the centre of the microphone 2.

The amplitudes of the forward waves and the backward waves, $p^+$and p^-, are:

$$p^+ = \frac{p_1 e^{ikx_1} - p_2 e^{ikx_2}}{e^{2ikx_1} - e^{2ikx_2}}; \tag{5}$$

$$p^- = \frac{p_1 e^{-ikx_1} - p_2 e^{-ikx_2}}{e^{-2ikx_1} - e^{-2ikx_2}}. \tag{6}$$

The transfer function for the incident wave alone H_I is:

$$H_I = \frac{P_{2I}}{P_{1I}} = e^{-ik(x_1 - x_2)} = e^{-iks} \tag{7}$$

where the separation between the two microphones $s = (x_1 - x_2)$.

Similarly, the transfer function for the reflected wave H_R is:

$$H_R = \frac{P_{2R}}{P_{1R}} = e^{ik(x_1 - x_2)} = e^{iks} \quad (8)$$

The transfer function for the total sound field is obtained using the sound pressures in two microphones:

$$H_{12} = \frac{P_2}{P_1} = \frac{e^{ikx_2} + R_c\, e^{-ikx_2}}{e^{ikx_1} + R_c\ e^{-ikx_1}}, \quad (9)$$

where R_c is the complex reflection coefficient of the material.

Rearranging Eq.(9) to yield the reflection coefficient R_c and using the incident and reflected wave transfer functions, the reflection coefficient can be written as:

$$R_c = \frac{H_{12} - H_I}{H_R - H_{12}} e^{2ikx_1} \quad (10)$$

Therefore, the normalized specific acoustic impedance of the panel absorber is:

$$Z = \frac{1 + R_c}{1 - R_c}, \quad (11)$$

while the absorption coefficient α is:

$$\alpha = 1 - |R_c|^2 \quad (12)$$

2.2 Absorption coefficients

Sound attenuating barriers are solid structures that intercept the direct noise transmission path from a sound source to a receiver. They reduce the noise level within the shadow zone on receptor side. Measurements of sound absorption were taken in a circular impedance tube with an internal diameter of 100 mm (see Figure 3). In keeping with a previous study of clamped poro-elastic plates [36], the experiments were conducted in accordance with the procedure outlined in BS EN ISO 10543-2:2001 [34], while the absorption coefficients are determined in accordance with EN ISO 354:2003 [35].

2.2.1 Methodology

A sample of test material with a movable rigid backing is placed at one end of a tube and a loudspeaker is placed at opposite end of the tube. Two ¼ inch microphones were mounted into a microphone grid at positions along the length of the impedance tube (as indicated in Figure 3), with each microphone grid being sealed tight to its housing. The microphones were fed to a four-channel data acquisition card (type MC3242, BSWA Tech.) which was connected to a computer for logging and further analysis. The acoustic sound field, an incident plane sinusoidal wave, P_i was created by a loudspeaker with a built-in amplifier. The transfer function method is used to determine the acoustical properties of the sample whereby the sound pressure at two fixed microphone locations within the tube is measured and then used as input for the acoustic transfer function to calculate the absorption coefficients.

2.2.2 Results

The measured absorption coefficient spectra for the three samples are shown in Figure 4. Specimen C01 has an initial absorption peak of 0.58 at 251 Hz and a secondary absorption peak of 0.55 at 630 Hz while specimen C02 has an absorption peak of 0.62 at 250 Hz and a secondary absorption peak of 0.45 at 800 Hz. Specimens C01 and C02 are effective at low and mid-frequency ranges and behave like porous panels. Specimen C03 has only one absorption peak

of 0.84 at 501 Hz. The absorption mechanism of specimen C03 is effective around the resonance frequency, thus it is behaving like a resonator. Specimen C03 attenuates 84% of acoustical energy impinging on its surface at its resonance frequency. Specimens C02 and C03 have the same nominal glass bead diameter (1–2 mm) but they have different thicknesses. Increasing the thickness of the materials enhanced the low frequency performance of the material while reducing mid-frequency absorption and shifting the resonance peak to a lower frequency. The resulting absorption performances of these samples are close to the peak sound pressure levels in the typical spectrum of road traffic noise.

2.3 Sound transmission loss

The sound transmission loss (TL) of acoustic materials is important in building acoustics and environmental noise attenuation panels. A modified impedance tube was employed previously [36] while following the procedure given in [34] for measuring transmission loss. The procedure described in [37,38] was adhered to in order to measure the transmission loss of the RGBP specimens.

2.3.1 Methodology

Measurements have been carried out in a circular impedance tube with an internal diameter of 100 mm (see Figure 5). A sample of test material is placed at the middle of a tube with a loudspeaker at one end and a rigid plate at the other. Six ¼ inch microphones (three microphones on each side of the test sample) were mounted into a microphone grid at positions along the length of the impedance tube. Each microphone grid was sealed tight to its housing. The microphones were fed to a four-channel data acquisition card (type MC3242, BSWA Tech.) which was connected to a computer for data analysis. The acoustic sound field, an incident plane sinusoidal wave P_i, was created by a loudspeaker that was fed with a power amplifier with a built-in pink noise generator (type PA50, BSWA Tech.). The sound signals at four fixed microphone locations within the tube were simultaneously measured. Microphones 1 and 3 for upstream tube and 4 and 6 for downstream tube are used to measure the transmission loss between 63 Hz and 500 Hz while microphones 2 and 3 for upstream tube, and 4 and 5 for downstream tube are used to measure the TL of noise barriers between 250 Hz and 1600 Hz. The VA_LAB using Transfer Function Method separates the incident and reflected energy from the measured transfer function, and then estimates the acoustic properties of the tested sample installed in the tube.

2.3.2 Determination of the transmission loss

The sound transmission loss of a noise barrier is defined [39] thus:

$$TL = 20\log\left|\frac{e^{jks}-H_{13}}{e^{jks}-H_{64}}\right| - 20\log|H_t| \qquad \text{for TL between 63–500 Hz} \qquad (13\,a)$$

$$TL = 20\log\left|\frac{e^{jks}-H_{23}}{e^{jks}-H_{54}}\right| - 20\log|H_t| \qquad \text{for TL between 250–1600 Hz} \qquad (13\,b)$$

where s is the distance between the centre of microphones, and k is the complex propagation constant, $H_{13} = \frac{P_3}{P_1}$ and , $H_{23} = \frac{P_3}{P_2}$ are the transfer function which is the ratio of the Fourier transform component between the sound pressures at microphones 1 and 3, and at microphones 2 and 3 respectively, and $H_{54} = \frac{P_4}{P_5}$, and $H_{64} = \frac{P_4}{P_6}$ are the transfer function which is the ratio of the Fourier transform component between the sound pressures at microphones 4

and 5, and at microphones 4 and 6. $H_t = \sqrt{|S_d/S_u|}$ is the ratio between the auto-spectrum in the upstream tube S_u and the auto-spectrum in the downstream tube S_d, respectively.

The transmission loss of three samples tested in the experiments are shown in Figure 6. The transmission losses of three samples increase throughout 1/3 octave band frequency range from 14.5 dB at 63 Hz up to 33.0 dB at 1600 Hz. At lower frequencies (63 Hz - 300 Hz) specimen C01 has a higher TL than specimens C02 and C03, while specimen C03 attenuates more noise than the other specimens at frequencies above 300 Hz. Specimens C01 and C02 have different nominal glass bead diameters but their transmission loss performance above 400 Hz is similar. The sound transmission losses of the specimens C01, C02 and C03 are 17.3 dB, 16.5 dB and 21.8 dB at 500 Hz, respectively.

These results are in the range of maximum transmission losses obtained with a practical noise barrier which is used for attenuating road traffic noise. The maximum noise transmission loss for noise barrier is approximately around 15 to 20 dB at 500 Hz for the barriers very close to either source side or receiver side. Using masses for a barrier in excess of around 15 kg/m^2 is a waste of recourses because the performance of noise barriers is limited by the diffraction over the top of the barrier and around the ends of the barriers [38].

When considering the use of the panels in a building structure, noise pollution limits prescribed by local authorities in the United Kingdom are typically 10 dB above the underlying level of noise [11]. Thus, the RGBPs tested are capable of insulating the occupants of a structure from such an adverse increase in environmental noise across all typical frequencies, performing particularly well at frequencies in excess of 500 Hz. This is of particular interest in the context of human occupancy since day-to-day residential and office space noise tends to occupy frequencies between 300 – 2000 Hz. It is noted that the 4–8 mm glass bead performs best at the lower end of this range.

3. Structural and mechanical experiments

In order to assess the suitability of RGBPs as structural components as well as noise barriers, an experimental campaign was conducted to determine the structural and mechanical properties of the panels. To this end, a series of tensile tests, compression tests and bending tests were conducted on various specimens in the Strengths of Materials laboratory at London South Bank University. In this section, the experiments are described, and the observed behaviour and the mechanical properties determined from the results are presented and discussed.

3.1 Determination of modulus of elasticity of fibreglass sheeting

Two tensile coupons were cut from full RGBP specimens in order to examine the behaviour of the facing material in situ. After determining the average breadth and thickness (23.1 mm, and 2.26 mm, respectively) across the central portion of the coupons, the ends were clamped in a Tinius Olsen H25KS tensile testing machine (see Figure 7), a clip gauge with a gauge length of 25 mm was attached to its central portion, and the specimen was then loaded in tension in the elastic range in order to determine the modulus of elasticity E_{fg}. Based on the four experiments conducted, an average value of E_{fg} = 7489 N/mm^2 was obtained.

3.2 Compression tests of recycled glass bead cores

Compression tests of cylinders cut from the panels were conducted at the Strengths of Materials laboratory at London South Bank University. In this section, the experiments are described and the load–deflection behaviour, the observed modes of failure, the ultimate resistances and the compressive strength of the cores are discussed.

After measuring their densities and conducting the acoustical experiments on them, the specimens shown in Figure 2 were tested in compression. Each specimen was positioned between the loading platens of a Zwick/Roell 250 kN Universal testing machine (see Figure 8) and then loaded in compression via displacement control at a rate of 5 mm/min. As can be seen in the graphs of machine load P against end shortening Δ shown in Figure 9, an initial regime of elastic deformation was observed in each test specimen prior to the onset of crushing of the bead core. There then followed a regime of successive crushing, cracking and compaction of the bead core. The failure modes observed are shown in Figure 10. It can be seen that the compressive resistances of the specimens are quite similar, indicating that the compressive strength $\sigma_{c,c}$ of both types of bead core are similar. Average compressive strengths are shown in Table 1 for the 1–2 mm bead core specimens and 4–8 mm bead core specimens, respectively. Although the compressive strength of the bead core is roughly 10% that of concrete, it should be noted that the material is approximately 12% as dense. Measurements of the compressive modulus of elasticity of the material were less reliable owing to the variable strain distribution being transferred through the bead core. It can be seen in the case of specimen C03-1-050 that after a certain amount of crushing of the bead core, the load increases again, which can be attributed to densification and compaction of the core after voids are removed. This indicates that an additional reserve of strength and resistance can be developed within recycled glass bead cores if the thickness of the core is optimised.

3.3. Bend testing of full panels

In this section, experiments where full RGBPs were loaded in bending are described and the load–deflection behaviour, the observed modes of failure and the ultimate loads are reported. These results are then used to determine some mechanical properties of the panels.

3.3.1 Specimens

The dimensions (nominal length L_{nom} × breadth b × depth h) and nominal bead diameters relating to the various specimens tested are shown in Table 2. Specimens were labelled in the manner shown in Table 2 in order to reflect the nominal diameter range of the glass bead (either 1–2 mm or 4–8 mm) and the type of panel specimen: L – long beam (L_{nom} = 2400 mm, b = 150 mm), S – short beam (L_{nom} = 1800 mm, b = 150 mm), P – panel (L_{nom} = 2400 mm, b = 450 mm). For example, specimen P11-1-S is a short beam with a core containing glass beads 1–2 mm in diameter. All specimens were 154 mm deep which includes the thicknesses of the two 2 mm fibreglass sheets. Measurements taken prior to testing indicate that the cut dimensions of the panel specimens were within 1% of the nominal dimensions shown in Table 2.

3.3.2 Apparatus and methodology

Four-point bending tests were carried out on the full panel specimens in order to simulate a constant bending moment across a portion of the panels so that the flexural stiffness and maximum bending moment resistance of the panels could be determined. The tests were conducted using the rig shown in Figure 11, which comprised a 500 kN capacity Zwick/Roell hydraulic loading jack, a loading table with adjustable supports, half-round contacts at the loading points situated at third points along the loaded span L of the specimen, a spreader bar,

a linear variable displacement transducer (LVDT) positioned underneath the specimen at midspan, and a data acquisition system. In order to accommodate some rotation at the ends of the beams, a 75 mm overhang was provided at both ends of the specimens, resulting in the tested spans being 150 mm shorter than the overall lengths of the specimens, as shown in Table 2. The tests were performed under displacement control at a crosshead displacement rate of 5 mm / min.

3.3.3 Results

In this section, the results obtained from the bending tests are discussed, namely, the load–deflection behaviour of the panels, the observed failure modes, the ultimate moments of the panels and the flexural modulus of the bead core.

3.3.3.1 Load–deflection behaviour

The influence of beam span and glass bead diameter on the behaviour of the panels is discussed in this section. The relationships between total applied load P and midspan deflection δ for all the panels tested are shown in Figure 12, with the curves forming groups based on the span and breadth of the specimens.

When examining the behaviour of the specimens, an initial period of elastic deformation is observed, which persists up until a certain level of strain whereupon some softening is observed owing to yielding of the polyurethane binding agent within the core on the tension side of the specimen – the value of this strain is dependent on the diameter of the glass beads in the core and the relative amount of binding agent present in the core (which was fixed at 7% by volume in all samples tested). Progressive yielding within the core leads to the core becoming largely ineffective in bending since shear transfer mechanisms are compromised. Finally, the specimens failed via a brittle cracking failure progressing rapidly from the tension side diagonally through the section of the panel towards the compression side of the bead core, with the fibreglass sheets remaining intact, as shown in the example of specimen P03-4-S in Figure 13 where separation of the facing sheet from the core can be observed on both the tension and compression sides of the panel. Compression side separation was present in only some of the specimens, whereas separation on the tension side was observed in all the specimens tested. The location of the shear failure was always at one of the point loads where the change in shear force is at a maximum for a beam in four-point bending. Upon examination of the specimens after failure, it was found that a thin layer of glass bead remained adhered to the fibreglass sheet (which is present in the example shown in Figure 13), indicating that the failure occurred within the polyurethane matrix binding the glass bead core as opposed to the adhesive itself. Thus, it is apparent that the failure mechanism is via debonding between the glass beads at the location of maximum longitudinal strain on the tension side, which eventually leads to the localised concentration of tensile stress underneath the point load causing a crack to propagate through the cross-section of the panel.

Given that the specimens were loaded in four-point bending with loads at third points, the bending moment across the central portion of the panels is $M = PL/6$. In Figure 14, the ultimate moments per metre width at the midspan of the panels, $M_{u,exp} / b$, which is relatable to strength, is plotted against the ratios of the midspan deflection at failure δ_{max} to L^3, since the specimens are loaded with point loads. The effective cross-sectional moment resistance of the panel sections is much the same for all specimens with values of $M_{u,exp} / b$ ranging from 18.1 kN m/m to 23.3 kN m /m and average values of 20.5 kN m/m and 21.3 kN m/m for the panels with glass bead diameters of 1–2 mm and 4–8 mm, respectively. However, when examining the values of δ_{max} / L^3, it can be seen that the 4–8 mm diameter glass bead cores fail at relatively larger

deflections and thus have a higher deformation capacity than those containing 1–2 mm diameter glass bead.

3.3.3.2 Effective flexural rigidity and mechanical properties

Examining the load–deflection behaviour of two typical panels, P02-4-S and P08-1-S, shown in Figure 15, it is clear to see that there is a level of load and deflection at which the flexural rigidity of the panel reduces owing to the onset of delamination between the bead core and the fibreglass sheet. It was found that the panels with 1–2 mm diameter glass bead cores maintained their elastic behaviour up to considerably larger deflections than those containing beads 4–8 mm in diameter, which is in agreement with the examples shown in Figure 15; it can also be seen that the initial elastic flexural rigidity is greater in specimen P08-1-S which contained 1–2 mm diameter glass bead. The gradient of the load–deflection curves, $\Delta P/\Delta\delta$, was used to assess the changing flexural behaviour of the panels qualitatively. The gradient at a particular point along the curve was calculated using a deflection differential $\Delta\delta = 0.25$ mm; the resulting curve was then smoothed by taking an average value of $\Delta P/\Delta\delta$ across an interval representing 0.25 mm of deflection. A comparison of typical raw and smoothed gradient curves is shown in Figure 16 for the example of specimen P08-1-S.

In the example of Figure 16, it can be seen that the load–deflection gradient is initially approximately constant which reflects the initial linear elastic behaviour of the specimen. At a particular level of deformation, the bead core begins to yield and soften on the tension side, which is represented by a progressive reduction in $\Delta P/\Delta\delta$ until it settles at a lower approximately constant value whereupon the bead core has lost efficacy. The effective flexural modulus $(EI)_{\text{eff}}$ of the composite section can be estimated by determining the change in the midspan deflection of a beam in four-point bending loaded at third points in accordance with Euler–Bernoulli beam theory, and rearranging for $(EI)_{\text{eff}}$:

$$(EI)_{\text{eff}} = \frac{23}{1296}\left(\frac{\Delta P}{\Delta\delta}\right)L^3 \tag{14}$$

In order to provide a qualitative assessment of how the efficacy of the core material is lost with increasing longitudinal bending strain, Eq.(14) is applied across the entire deformation regime of the panels. It is noted that, after yielding and especially in the very final stages of the tests when large cracks propagate through the bead core, the neutral axis shifts upwards towards the compression side of the panel, and thus the validity of Eq.(14) is compromised. It was observed that the integrity of the fibreglass sheets was maintained throughout the experiments, with the sheets deforming in an elastic manner with a constant modulus of elasticity E_{fg}, which is taken as 7489 N/mm^2 based on the tensile tests discussed in Section 3.1. The effective modulus of elasticity of the glass bead core, E_{c}, is determined thus:

$$E_{\text{c}} = \frac{(EI)_{\text{eff}} - 2E_{\text{fg}}I_{\text{fg}}}{I_{\text{c}}} \tag{15}$$

where I_{fg} and I_{c} are the second moments of area of a single fibreglass sheet and the bead core, respectively. In all specimens, I_{fg} and I_{c} were calculated using the nominal fibreglass sheet thickness $t_{\text{fg}} = 2$ mm and the depth of the bead core $h_{\text{c}} = 150$ mm; measurements of these values before the individual tests showed a variance of less than 1% when compared to the nominal values. Again, it is noted that the estimate for E_{c} described in Eq.(15) is fully valid only up until the effective flexural rigidity begins to reduce owing to the onset of tension-side softening. Nevertheless, applying Eq.(15) across the full deformation regimes provides at least a

qualitative assessment of the efficacy of the bead core after yielding has commenced. In Figure 17, the difference between the effective moduli E_c determined for panel specimens P02-4-S and P08-1-S can be seen; the average initial linear elastic moduli $E_{c,el}$ are 881 N/mm^2 and 1159 N/mm^2, respectively, reflecting the higher stiffness of the 1–2 mm diameter glass bead core. The effective elastic modulus decreases after yielding initiates and the bead core becomes practically ineffective in the latter portion of the experiments. It can be seen that the 1–2 mm diameter glass bead core maintains its elastic stiffness noticeably longer than the 4–8 mm diameter bead core; however, the 4–8 mm bead core loses its stiffness more gradually and exhibits somewhat greater ductility.

The maximum stress and strain in the bead core, $\sigma_{c,max}$ and $\varepsilon_{c,max}$, respectively, can be calculated by assuming a linearly-varying longitudinal strain across the entire depth of the composite section centred at the neutral axis. The maximum strain occurring in the glass bead core at given applied moment M is:

$$\varepsilon_{c,max} = \frac{Mh_c}{2(EI)_{eff}}, \tag{16}$$

while the maximum stress is:

$$\sigma_{c,max} = \varepsilon_{c,max} E_c \tag{17}$$

Typical stress–strain relationships in bead cores with glass bead of different diameters are shown in Figure 18 for specimens P02-4-S and P08-1-S. The curves are truncated after the attainment of the ultimate stress since the validity of the application of Eqs.(16) and (17) is compromised beyond this point: progressive softening of the bead core on the tension side of the panels causes the neutral axis of the section to move closer to the fibreglass sheet in compression. Overall, it can be seen that the 1–2 mm diameter glass bead core is stronger and stiffer than the 4–8 mm diameter bead core, although the 4–8 mm diameter bead core is noticeably less brittle and can accommodate considerably higher strains prior to the core losing efficacy. Examining the curves, it is found that the proportional limit stress $\sigma_{c,el}$ of the bead core in specimen P08-1-S is 1.56 N/mm^2, while the ultimate stress $\sigma_{c,u}$ = 1.80 N/mm^2; it is noted that these values are lower than the values for compressive strength discussed in Section 3.2, which indicates that failure does indeed initiate on the tension side of the specimens. For specimen P02-4-S, $\sigma_{c,el}$ = 1.02 N/mm^2, while $\sigma_{c,u}$ = 1.23 N/mm^2. The elastic limiting strain $\varepsilon_{c,el}$ is taken as the strain coinciding with $\sigma_{c,el}$, which is 0.129% and 0.137% for specimens P02 and P08, respectively. The ultimate strain $\varepsilon_{c,u}$, i.e., the strain coinciding with the ultimate stress, is 0.312% and 0.189% for specimen P02-4-S and specimen P08-1-S, respectively; these values are comparable to failure strains observed in concrete. The value of $\varepsilon_{c,u}$ /$\varepsilon_{c,el}$ provides an indication of the ductility of the core material, which is 2.41 for specimen P02-4-S and 1.38 for specimen P08-1-S, again demonstrating the greater deformation capacity of the 4–8 mm diameter glass bead core.

A summary of the calculated values of $E_{c,el}$, $\varepsilon_{c,el}$, $\sigma_{c,el}$, $\varepsilon_{c,u}$ and $\sigma_{c,u}$ for all the specimens tested is shown in Table 3 along with average values and coefficients of variation (COV) for each property determined for the two different glass bead cores. Upon inspection of these average values, it can be seen that, in agreement with the particular examples shown in Figures 15, 17 and 18, the 1–2 mm diameter glass bead core is stiffer and stronger, but less ductile, than 4–8 mm diameter glass bead core; a moderate amount of variance was observed in these measurements, as evidenced by the values of COV shown in Table 3. As was also shown in Figure 17 when examining the effective stiffness of the panels, the elastic stiffness of the 1–2 mm diameter glass bead cores was maintained up to a higher strain than that of the 4–8 mm

diameter glass bead core, with average values of $\varepsilon_{c,el}$ of 0.135% and 0.106%, respectively. After yielding initiates, cores containing 4–8 mm diameter glass beads are considerably more ductile, with an average value of $\varepsilon_{c,u}/\varepsilon_{c,el}$ of 3.27 compared to an average of 1.35 for the 1–2 mm diameter bead cores.

Some trends amongst these mechanical properties can be observed upon examination of Figures 19 to 21. It can be seen in Figure 19 that there is a positive correlation between the elastic stiffness $E_{c,el}$ and the proportional limit stress $\sigma_{c,el}$ of the glass bead cores, with the 1–2 mm diameter glass bead cores being stiffer and stronger than the 4–8 mm diameter glass bead cores. In Figure 20, it can be seen that there is a clear correlation between $\sigma_{c,u}$ and $\sigma_{c,el}$, and again that the 1–2 mm diameter glass bead cores are stronger than the 4–8 mm diameter glass bead cores. Finally, in Figure 21, it can be seen that the 4–8 mm diameter glass bead cores are overall more ductile than the 1–2 mm diameter glass bead, although it is noted that the variances of ε_{el} and ε_{u} are relatively small for the 1–2 mm diameter glass bead cores, while the variance of ε_{el} is considerably larger for the 4–8 mm diameter glass bead cores.

3.4 Design of recycled glass bead panels in bending

The values reported in Table 3 are used to provide mechanical properties to inform the preliminary design of structural RGBP members. It is emphasised that a full reliability analysis of the cross-sectional resistance of recycled glass bead panels, based on a corpus of experimental results varying other properties such as panel depth, must be conducted prior to the use of such properties in structural design; the purpose of the current section is to provide an initial indication of the suitability of RGBP members in structural applications.

The current approach assumes that the panels are to be assessed in an ultimate limit state (ULS) and thus the values of ultimate strength $\sigma_{c,u}$ are to be used in design. It is proposed to use the proportional limit strength $\sigma_{c,el}$ when assessing the serviceability of the panels in order to preclude permanent damage and to limit deflections. Since the fibreglass sheets do not approach their ultimate strength of approximately 300 N/mm^2, it is more appropriate to estimate the stress in the fibreglass by assuming strain compatibility at the interface between the bead core and the fibreglass sheets. Assuming a plastic stress block at failure owing to redistribution of bending stresses and ignoring higher order terms, the moment of resistance of the RGBPs can be taken as:

$$M_{\mathrm{R}} = b\left(\frac{\sigma_{\mathrm{c,u}} h_{\mathrm{c}}^2}{4} + E_{\mathrm{fg}}\varepsilon_{\mathrm{c,u}} h_{\mathrm{c}} t_{\mathrm{fg}}\right) \tag{18}$$

In Figure 22, a comparison is made between the experimental values of ultimate moment $M_{u,exp}$ and the theoretical moments of resistance M_R, which have been calculated using the measured values of $\sigma_{c,u}$, $\varepsilon_{c,u}$ and E_{fg}. A full reliability analysis is recommended in order to determine appropriate design values of these properties for use in conjunction with partial factors calibrated according to reliability-based methods such as those described in the European structural design standard EN 1990 [40]. As can be seen in Figure 22, the moments of resistance determined using Eq.(18) are safe-sided and conservative, with average values of $M_{u,exp}$ / M_R of 1.57 and 1.52 for the 1–2 mm diameter glass bead cores and the 4–8 mm diameter glass bead cores, respectively. Further investigation of the distribution of stresses within the fibreglass sheets and bead core can provide a more accurate estimation of the moment of resistance.

In order to demonstrate the feasibility of employing RGBPs as a flooring system in practice, a sample of exemplar span tables have been produced, with achievable spans (in m) shown in Tables 4 and 5 for the cases of 1–2 mm diameter bead core and 4–8 mm diameter bead core, respectively. In order to determine M_R from Eq.(18), the average values of $\sigma_{c,u}$ and $\varepsilon_{c,u}$ shown

in Table 3 have been used. A characteristic permanent action g_k = 1.5 kN/m^2 is included in order to account for additional actions such as finishes and services. The partial factors for permanent actions γ_G and variable actions γ_Q taken as 1.35 and 1.50, respectively, in accordance with EN 1990 [40]. Assuming simply-supported end conditions, the applied design moment is thus

$$M_{Ed} = (\gamma_G g_k + \gamma_Q q_k) L^2/8 \quad (19)$$

The achievable spans are found by solving $M_R = M_{Ed}$ for L. The results for the achievable spans shown in Tables 4 and 5 indicate that RCGP floor panels are suitable for typical spans encountered in practice under loadings that would be expected in commercial and residential developments. Such panels could be supported on the wider bottom flanges of asymmetric beams, thus creating a lightweight and shallow floor system in practice. It is stressed that, in addition to performing experiments on specimens with core depths across the full range shown in Tables 4 and 5, a full reliability analysis of a design method based on Eq.(18) must be conducted prior to recommending the use of such panels in practice, particularly with regard to calibrating a material partial factor accurately.

3.4.1 Comparison with conventional flooring systems

When comparing the structural performance of the 150 mm-deep panels examined in the current study to conventional flooring systems, the achievable spans are comparable to i) 50 – 100 mm hollowcore concrete floors [41] while being approximately 60% lighter, ii) a 60 – 125 mm ComFlor composite floor systems [42] while being approximately 40% lighter, or iii) a 50–120 mm deep light-gauge steel floor joist system [43] without requiring additional thermal or acoustic insulation. Thus, a floor system comprising RGBPs is considerably lighter than concrete and with better thermal and acoustic performance than lightweight steel floor systems; this demonstrates the multifunctional benefits of the RGBP floor system.

4. Conclusions and further work

An investigation has been conducted to determine the acoustical and structural parameters of recycled glass bead panels comprising two fibreglass facing sheets surrounding an inner core of recycled glass beads bonded in a matrix of polyurethane resin.

The acoustical experiments were conducted on cylindrical samples cut from full panel specimens in an impedance tube using the transfer function method in order to determine the sound absorption coefficient and transmission loss of them. The results show that the thicker samples attenuated noise more effectively at lower frequencies while the thinner sample was better at absorbing sound at mid-frequency (around its own natural frequency). The absorption performances of the panels were found to be close to the peak sound pressure levels in the typical spectrum of road traffic noise. The sound transmission loss of the samples measured at 500 Hz are in the range of maximum transmission loss obtained with a practical noise barrier, hence demonstrating the efficacy of the panels in providing acoustical insulation both as highway noise barriers and also in a building structure.

Tensile tests were performed on coupons cut from the fibreglass outer sheets of full recycled glass bead panels in order to determine the elastic modulus of the sheeting material after the fabrication process. Compressive testing was conducted in order to determine the compressive strengths of the two bead core mixes under investigation. It was found that the compressive strengths of cores containing 1–2 mm diameter bead and those containing 4–8 mm diameter bead were very similar. It was also found that, after complete compaction of the thinner sample,

the overall load increased again, indicating that there exists an additional reserve of strength within recycled glass bead cores.

Four-point bending tests were conducted on full recycled glass bead panels of various spans, widths and glass bead core mixes. The results for applied load and midspan deflection were used to determine the strength, stiffness and ductility of the bead cores. It was found that the 1–2 mm diameter glass bead core was stiffer and stronger but less ductile than the 4–8 mm diameter glass bead core. An initial design equation for the cross-sectional moment resistance was proposed; it was found that it provided conservative and safe-sided predictions when compared to the experimental results. It was then shown that, when extrapolating the results obtained for panels with a core depth of 150 mm across a wider range of depths, floor spans comparable to those achievable by lightweight concrete, steel or composite floor systems are possible. Thus, when considering the combined structural and acoustical performance of the panels, there is potential for their multifunctional application within both building structures and as stand-alone noise barriers.

It is recommended that further bending tests to be conducted in order to inform a complete reliability analysis of recycled glass bead panels in bending, especially on panels of varying depths. In addition, in the context of applying the panels in external and exposed conditions, tests on samples subjected to accelerated aging will be beneficial in assessing their long-term resilience. For panels that may be subjected to cyclic or dynamic loadings, e.g. wind loads, a series of fatigue and vibrational testing is recommended.

5. Acknowledgements

This work was supported by London South Bank University Acoustics and the CCiBSE research centre. The authors wish to extend their gratitude to Mr Paul Elsdon and Mr Graham Bird of the Strengths of Materials laboratory for their expertise and dedication in conducting the structural and mechanical experiments, and to Professor Stephen Dance for his assistance with the acoustical experiments. Special thanks is also expressed to Mr Ahmad Seedat for his help in conducting the structural experiments.

References

1. Department for Communities and Local Government, 2012. National Planning Policy Framework. Department for Communities and Local Government.
2. Highways England, 2017. Design manual for roads and bridges. Guildford: Highways England, 2017.
3. Ministry of Housing, Communities and Local Government. 2017. Fixing our broken housing market. London: HM Government, 2017.
4. J. Hong, G.Q. Shen, Z. Li, B. Zhang, W. Zhang. 2018. Barriers to promoting prefabricated construction in China: a cost–benefit analysis, *Journal of Cleaner Production*, 172:649–660.
5. M.M. Fard, S.A. Terouhid, C.J. Kibert, H. Hakim. 2017. Safety concerns related to modular/prefabricated building construction, *Int. J. Inj. Contr. Saf. Promot.*, 24(1):10–23.
6. R. Jin, S. Gao, A. Cheshmehzangi, E. Aboagye-Nimod. 2018. A holistic review of off-site construction literature published between 2008 and 2018, *Journal of Cleaner Production*, 202:1202–1219.
7. W. Pan, R. Sidwell. 2011. Demystifying the cost barriers to offsite construction in the UK, *Construction Management Economics*, 29(11):1081–1099.

8. Z. Li, G.Q. Shen, X. Xue. 2014. Critical review of the research on the management of prefabricated construction. *Habitat Int.,* 43 (2014), pp. 240-249.
9. V.W.Y. Tam, I.W.H. Fung, M.C.P. Sing, S.O. Ogunlana. 2015. Best practice of prefabrication implementation in the Hong Kong public and private sectors, *Journal of Cleaner Production*, 109 (2015), pp. 216-231.
10. M.R. Hosseini, I. Martek, E.K. Zavadskas, A.A. Aibinu, M. Arashpour, N. Chileshe. 2018. Critical evaluation of off-site construction research: a Scientometric analysis, *Autom. Construct*., 87:235-247.
11. Department for Environment Food and Rural Affairs (DEFRA). 2013. Draft Noise Action Plan: Railways (Including Major Railways) Environmental Noise (England) Regulations 2006, as amended.
12. Department for Communities and Local Government (DCLG) (2006). Planning policy guidance 24: planning and Noise.
13. T. S. Serniabat, M. N. N. Khan, M. F. M. Zain. 2014. Use of Waste Glass as Coarse Aggregate in Concrete: A Possibility towards Sustainable Building Construction, *International Journal of Civil and Environmental Engineering* Vol:8, No:10, 2014.
14. A. Mohajerani, J. Vajna, T. Ho, H. Cheung, H. Kurmus, A. Arulrajah, S. Horpibulsuk. 2017. Practical recycling applications of crushed waste glass in construction materials: A review, *Construction and Building Materials*, 156:443–467,
15. J. Tao. 2017. Use of Crushed Recycled Glass in the Construction of Local Roadways. Ohio's Research Initiative for Locals, The Ohio Department of Transportation Office of Statewide Planning and Research, Technical Report 135329.
16. I. Demir. 2009. Reuse of waste glass in brick production. *Waste Management & Research*, 27:572–577.
17. R. Stewart. 2011. 'Composites in construction advance in new directions', *Materials Today*, 6 September 2011.
18. C. Jofeh. 2016. 'Strength and durability of glass', in M. Forde (ed.), *ICE Manual of Construction Materials*, London: Institution of Civil Engineers, 807–812.
19. H. Aygün, F. McCann. 2019. Investigation of acoustical and structural parameters of recycled glass bead composite panels. Inter-Noise 2019 - the 48th International Congress and Exhibition on Noise Control Engineering. Madrid, Spain 17–21 June 2019
20. M. Tascan, K. Lyon Gaffney. 2012. Effect of Glass-Beads on Sound Insulation Properties of Nonwoven Fabrics, *Journal of Engineered Fibres and Fabrics*, 7(1):101–105.
21. H. Heriyanto, F. Pahlevani, V. Sahajwalla, 2018. From waste glass to building materials – An innovative sustainable solution for waste glass, *Journal of Cleaner Production*, Volume 191, 2018, Pages 192–206.
22. A-H. I. Mourad, A. H. Idrisi, M. C. Wrage, B. M Abdel-Magid. 2019. Long-term durability of thermoset composites in seawater environments, *Composites Part B*, 168:243–253.
23. L. Cong, F. Yang, G. Guo, M. Ren, J. Shi, L. Tan. 2019. The use of polyurethane for asphalt pavement engineering applications: A state-of-the-art review, *Construction and Building Materials*, 225:1012–1025.
24. U. Sandberg, 2003. The Multi-Coincidence Peak around 1000 Hz in Tyre/Road Noise Spectra. Euronoise Naples.
25. G.G. Fleming. 1994. Performance Evaluation of Experimental Highway Noise Barriers, technical report FHWA-RD-94-093. US Federal Highway Administration, 1994.

26. J. Allard and N. Atalla, 2009. Propagation of Sound in Porous Media: modelling sound absorbing materials. 2nd edition. Wiley: Chichester.
27. K. Polcak, R.J. Peppin. 2010. Case study: Reflective and Non-Reflective Highway Barriers, technical report: TRB ADC 40 Summer Meeting, Denver, CO, 2010.
28. H. W. Lord, W. Gatley and H. Evenson, 1980. *Noise Control for Engineers.* London: McGraw Hill.
29. T. D. Rossing, 2007. Springer Handbook of Acoustics, p.127.
30. B. Kotzen, C. English. 2009. *Environmental noise barriers: a guide to their acoustic and visual design.*2nd Edition. Oxon: Taylor and Francis.
31. V. Dravitzki, D. K. Walton, W. B. Wood. 2006. "Determining the influence of New Zealand road surfaces on noise levels and community annoyance," Land Transport New Zealand, Wellington Report 292.
32. R. R. Boullosa, A. P. Lopez. 1987. Technical Note: traffic noise spectra in dry and wet street conditions, Noise Control Engineering Journal, 1987, 29(2), 45-54.
33. International Standards Organisation. 1998. BS EN 1793-3:1998 *Acoustics – Road traffic noise reducing devices – Test method for determining the acoustic performance. Part 3: Normalised traffic noise spectrum.*
34. International Standards Organisation. 2001. BS EN ISO 10543-2:2001. *Acoustics – determination of sound absorption coefficient and impedance in impedance tubes. Part 2: Transfer-function method.* London: British Standards Institute.
35. International Standards Organisation. 2003. BS EN ISO 354:2003 *Acoustics — Measurement of sound absorption in a reverberation room*. London: British Standards Institute.
36. H. Aygun, K. Attenborough, 2008. Sound absorption by clamped poro-elastic plates. *The Journal of the Acoustical Society of America*, 124, 1550-1556.
37. J. S. Bolton., R. J. Yun, J. Pope, D. Apfel, 1997. Development of a new sound transmission test for automotive sealant materials. *Proc. ASE*, Paper 971896.
38. J. Y. Chung, D. A. Blaser, 1980. Transfer function methods of measuring in-duct acoustic properties. II Experiment. *The Journal of the Acoustical Society of America* 68, 914.
39. R. S. Peters, B. J. Smith, M. Hollins. 2011. Acoustics and Noise Control. 3rd edition. Pearson.
40. Comité Européen de Normalisation. 2002. *EN 1990:2002 Eurocode – Basis of structural design*, CEN, 2002.
41. FP McCann Ltd. 2019. Precast Flooring Solution (technical guide). FP McCann: 2019.
42. Tata Steel. 2017. ComFlor® manual - Composite floor decking design and technical information (technical guide). Tata Steel UK Ltd: London, 2017.
43. Metsec. 2011. Z and C-sections for building shell and mezzanine floor applications (technical guide). Metsec: 2011.

Figure 1: Sample of recycled glass bead panel.

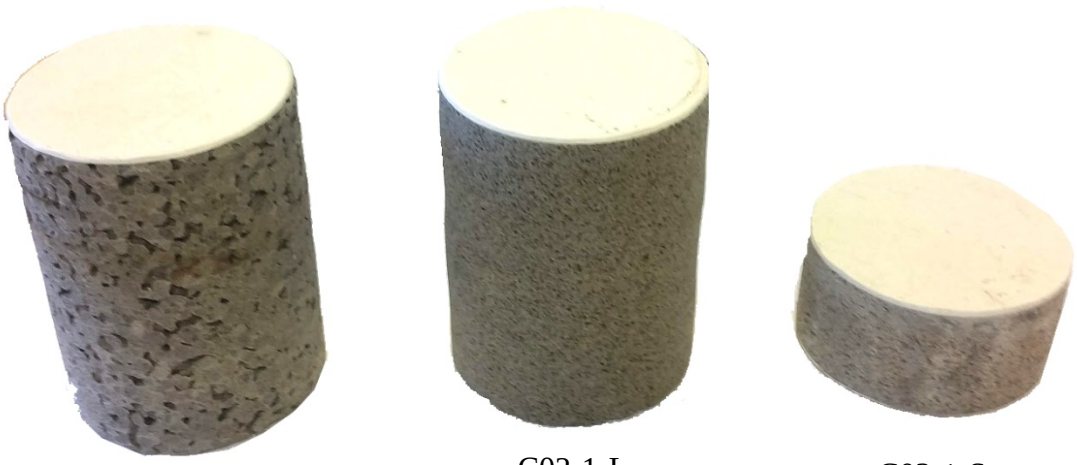

Figure 2: Acoustical and compression test samples.

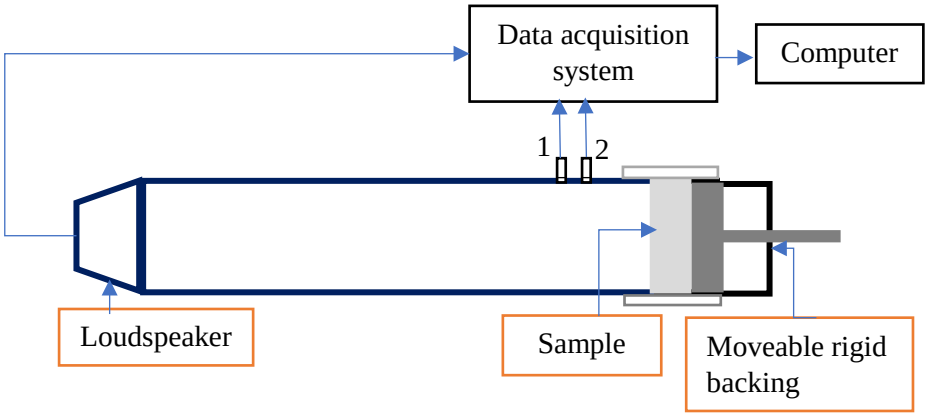

Figure 3: Impedance tube system for absorption measurement.

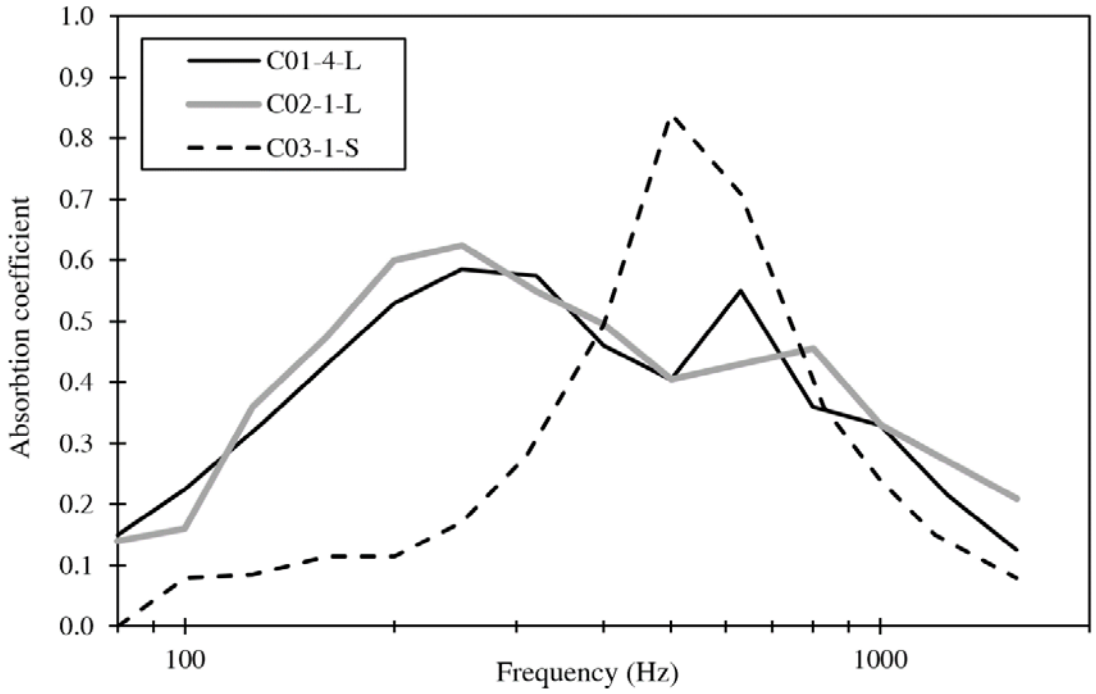

Figure 4: Absorption coefficient of glass bead samples.

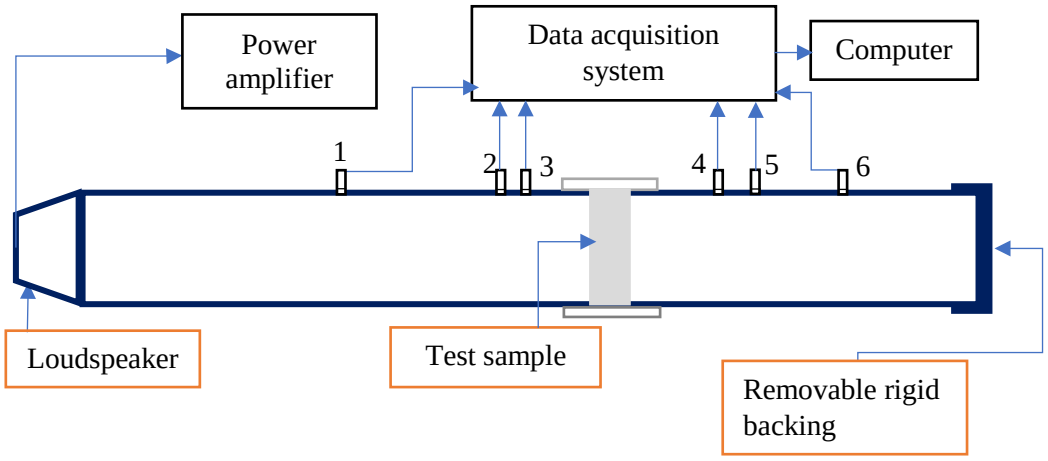

Figure 5: Impedance tube system for transmission loss measurement.

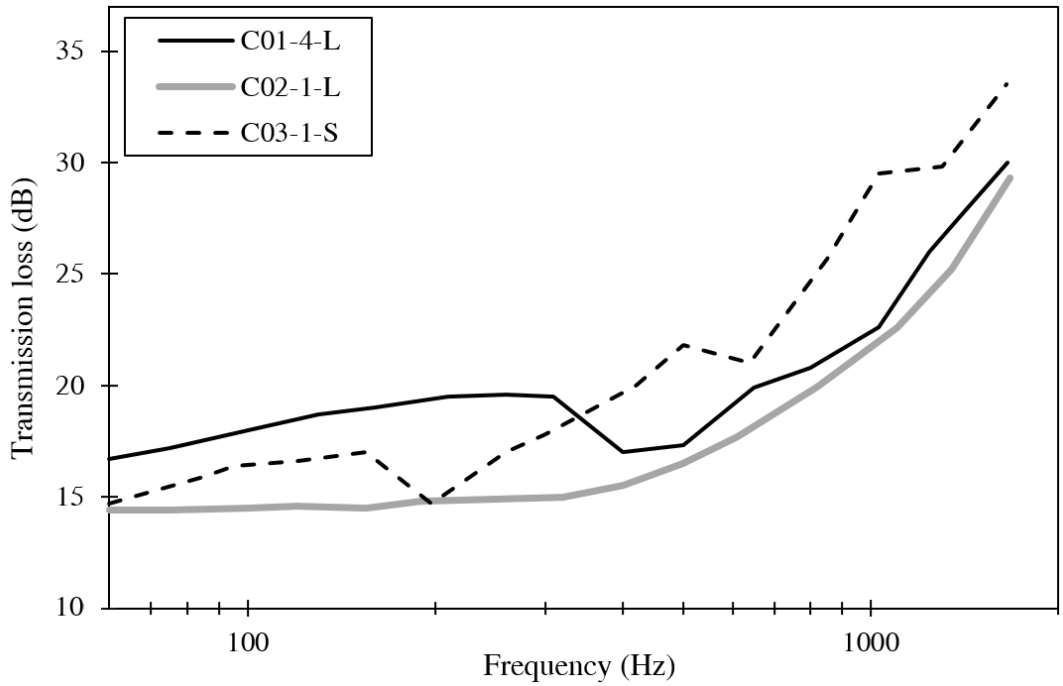

Figure 6: Transmission loss of glass bead samples.

Figure 7: Fibreglass specimen clamped in preparation for determination of modulus of elasticity.

Figure 8: Specimen C02-1-L positioned in preparation for compression testing.

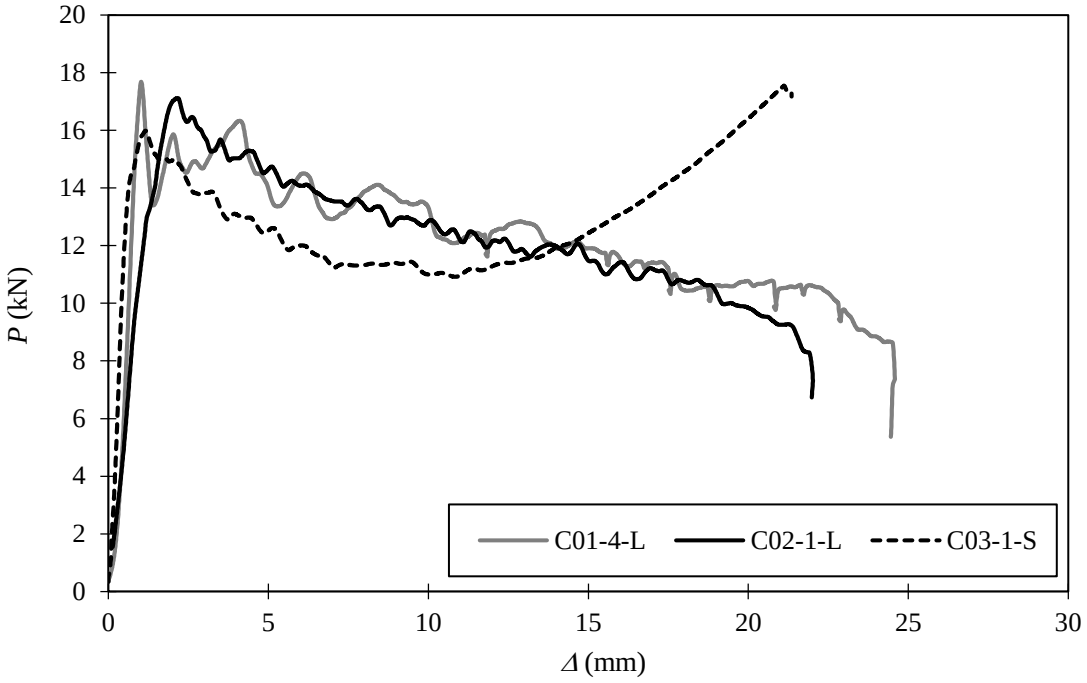

Figure 9: Load–end shortening relationships of recycled glass bead cores in compression.

Figure 10: Failure modes of glass bead core specimens in compression: (left to right: specimens C01-4-L, C02-1-L, C03-1-S).

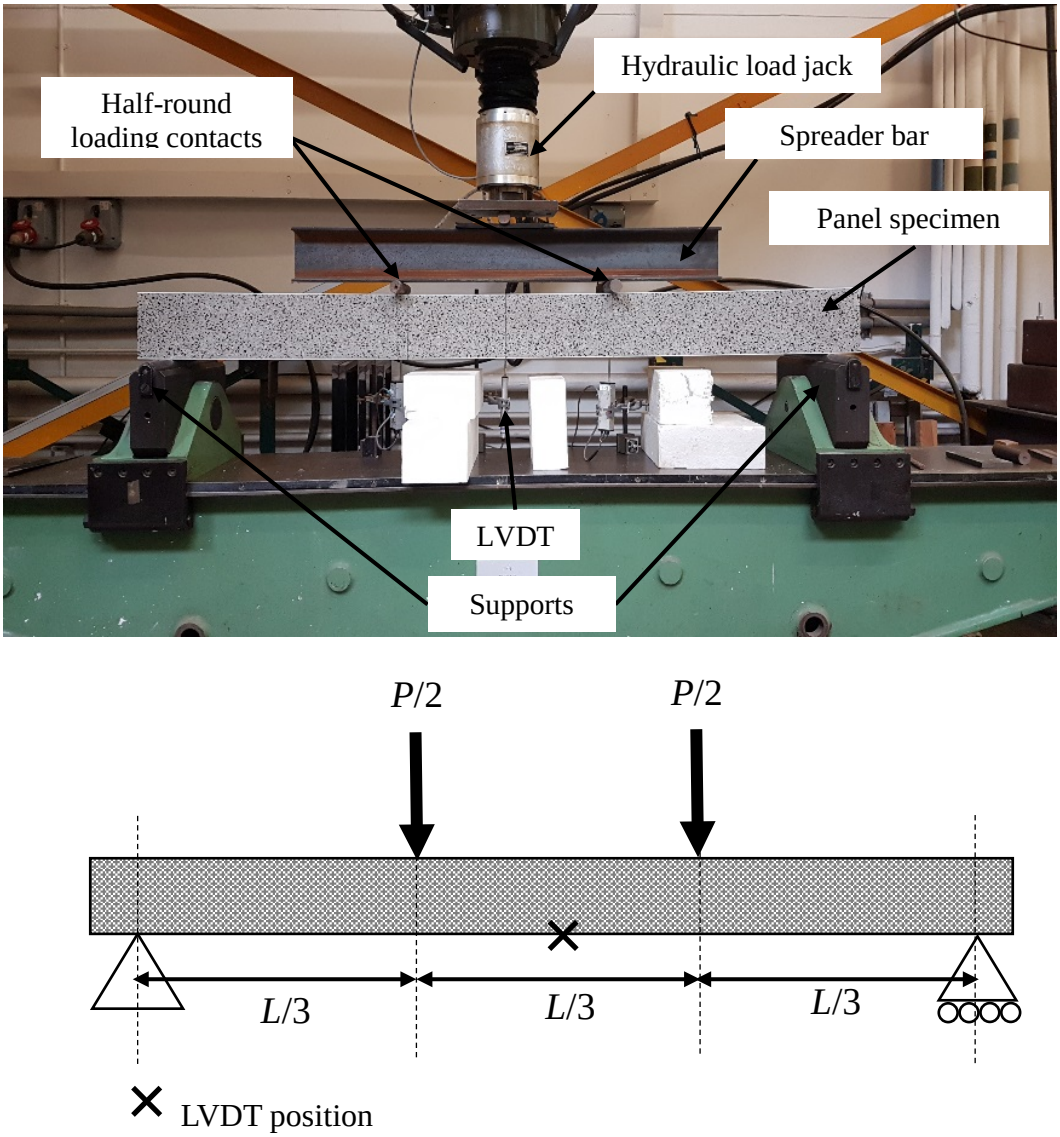

Figure 11: Loading rig used for four-point bending tests.

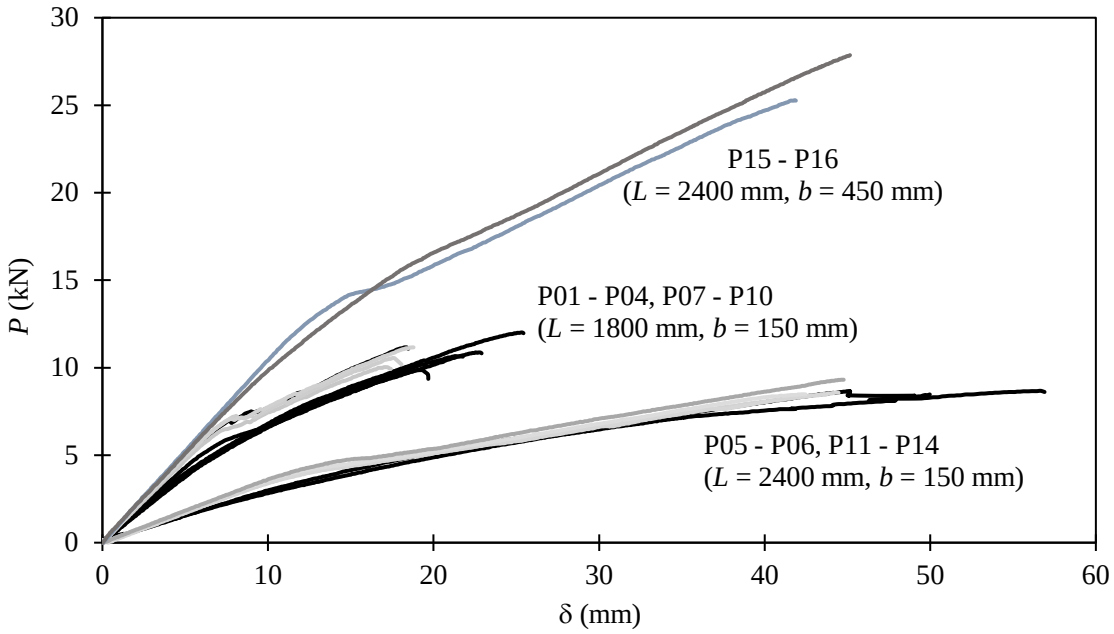

Figure 12: Load – deflection curves for the composite panels tested in bending.

Figure 13: Typical example of shear failure through bead core (specimen P03-4-S).

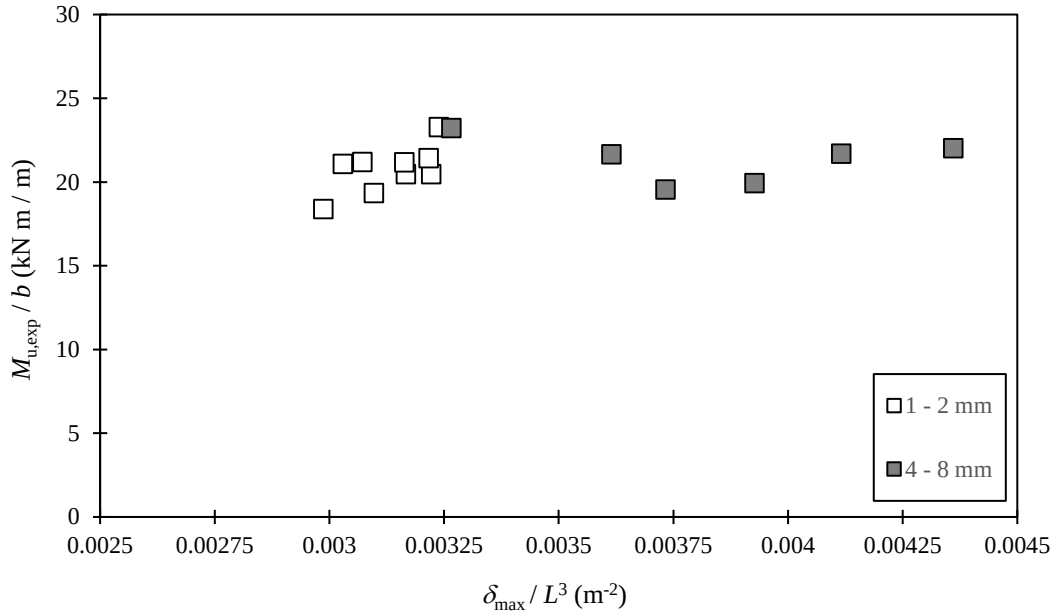

Figure 14: Plot of ultimate moments per metre width against ratios of span to maximum deflection for composite panels.

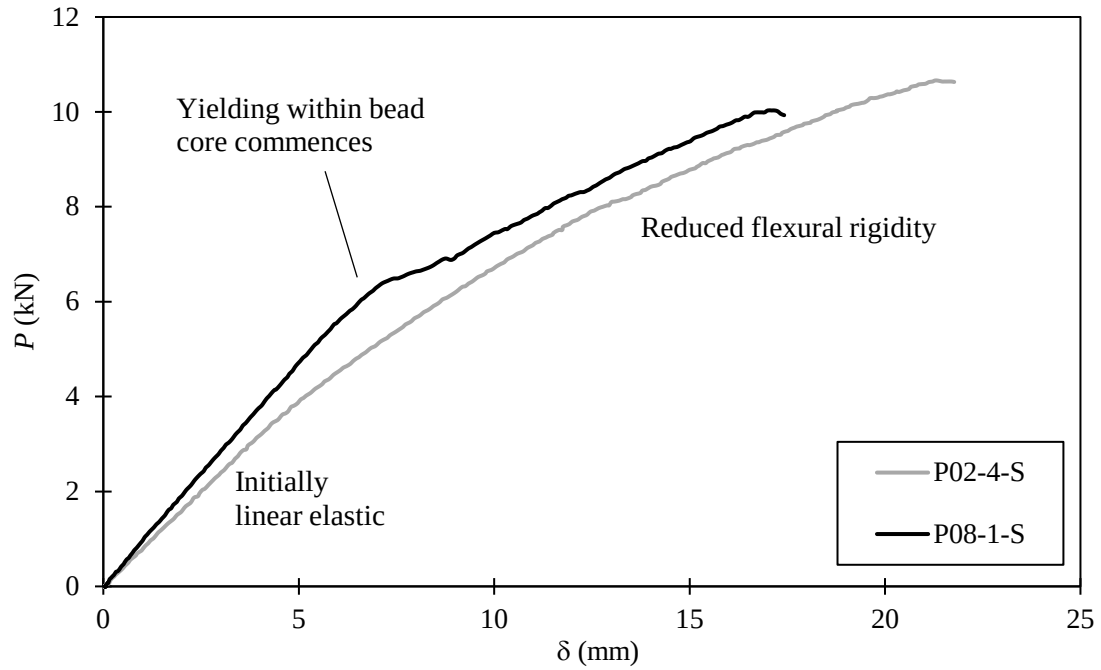

Figure 15: Load – deflection curves for specimens P02-4-S and P08-1-S, exhibiting reduction in flexural rigidity owing to delamination.

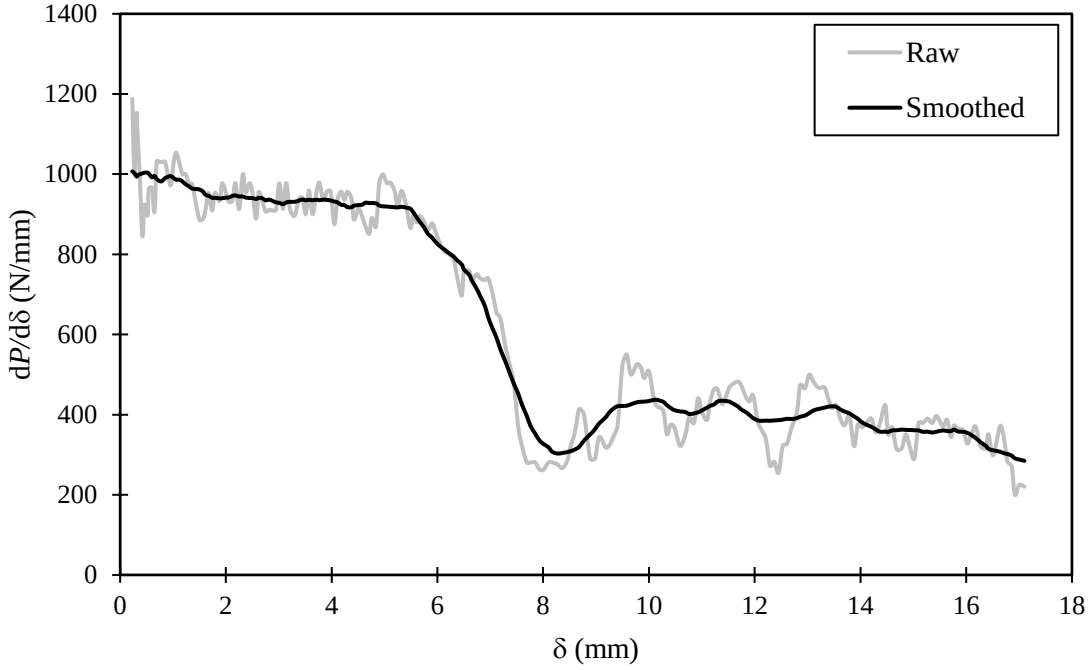

Figure 16: Typical comparison of raw and smoothed $\Delta P/\Delta\delta$ curves (specimen P08-1-S).

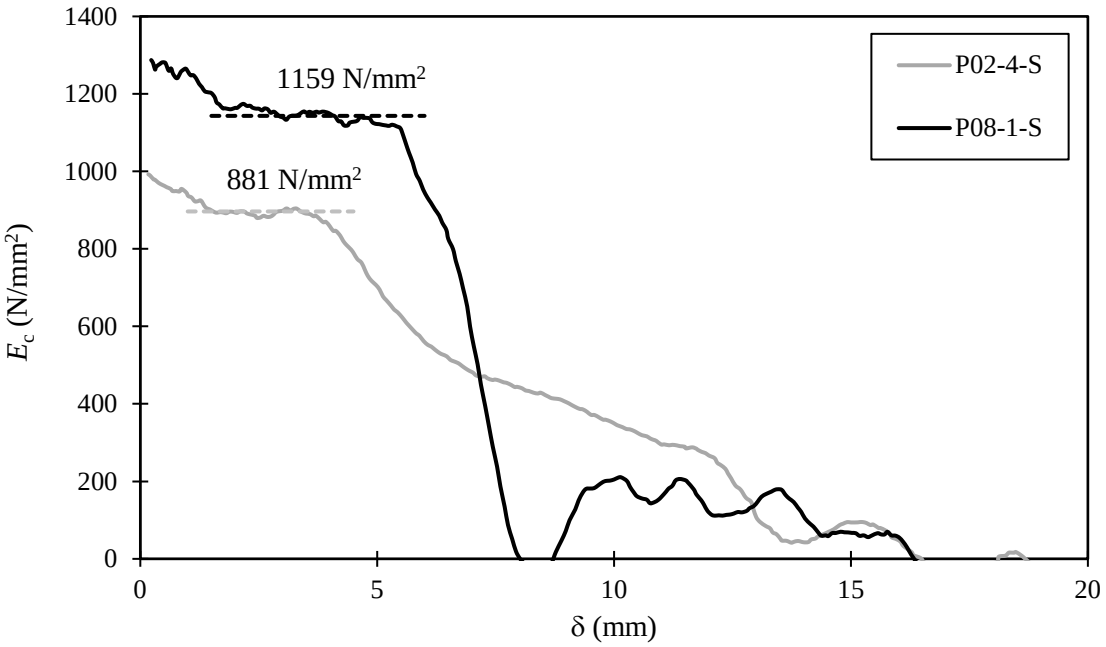

Figure 17: Comparison of effective modulus of bead cores with different glass bead diameters.

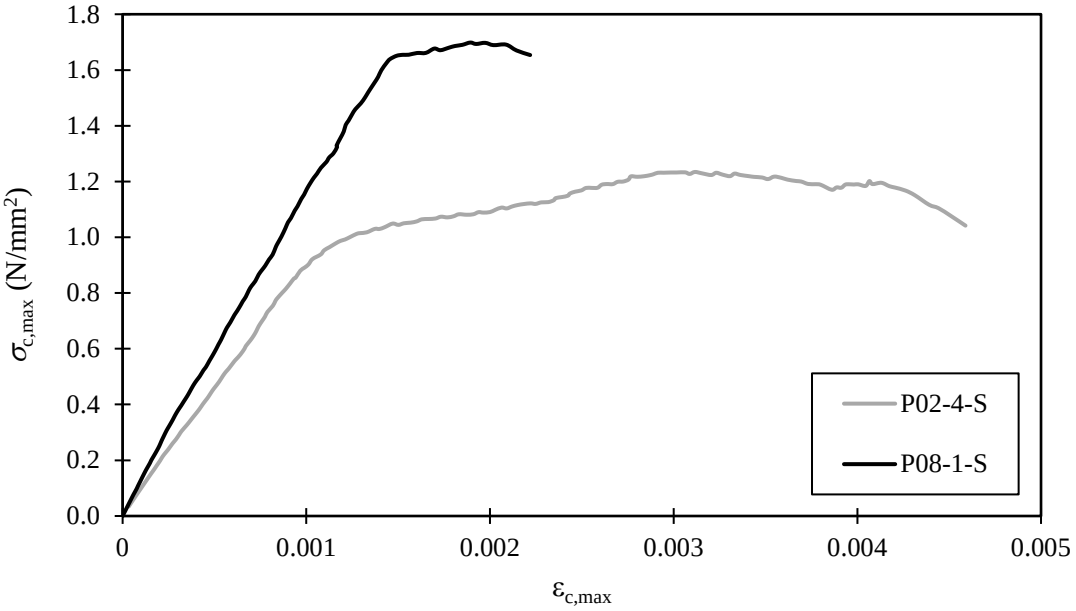

Figure 18: Comparison of stress–strain relationships in bead cores with different glass bead diameters.

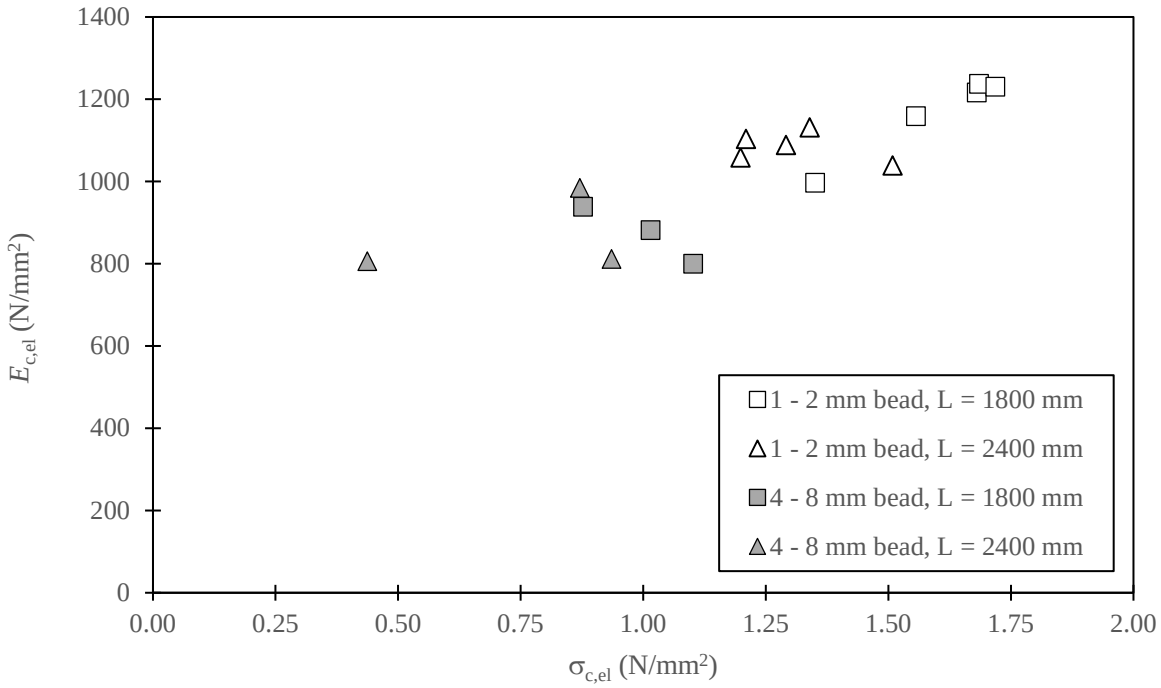

Figure 19: Comparison of values of $\sigma_{c,el}$ and $E_{c,el}$ for glass bead cores.

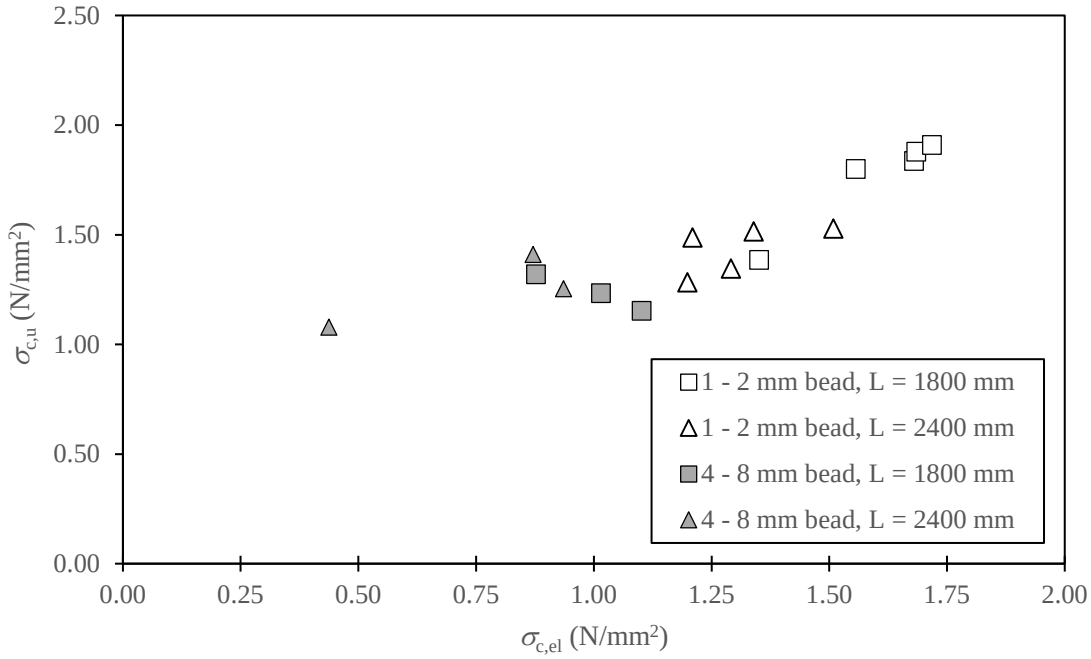

Figure 20: Comparison of values of σ_{el} and σ_u for glass bead cores.

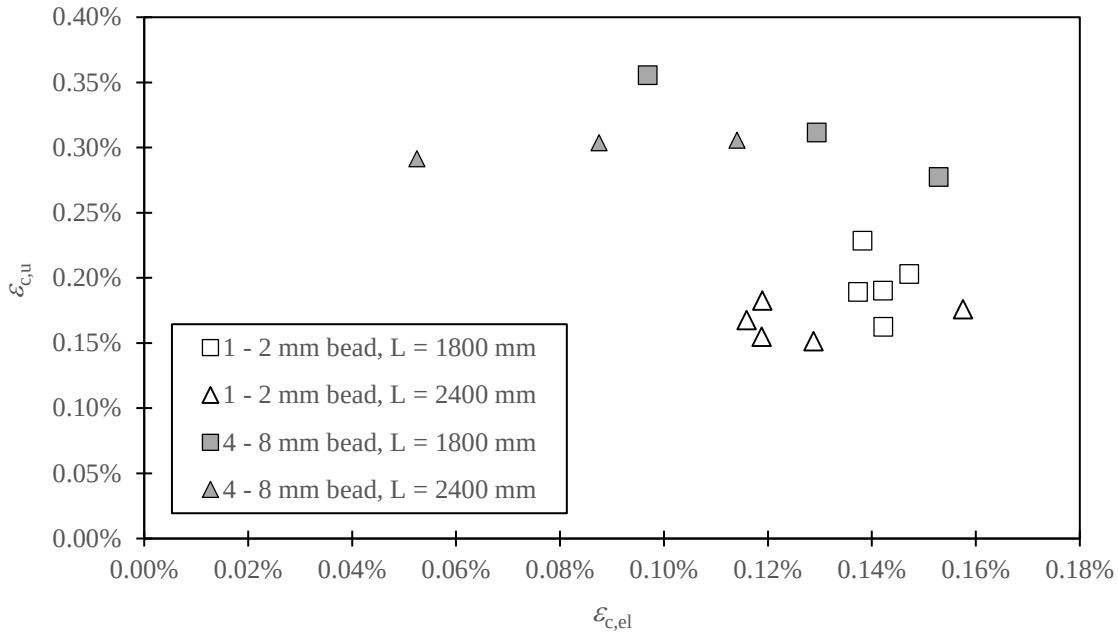

Figure 21: Comparison of values of $\varepsilon_{c,el}$ and $\varepsilon_{c,u}$ for glass bead cores.

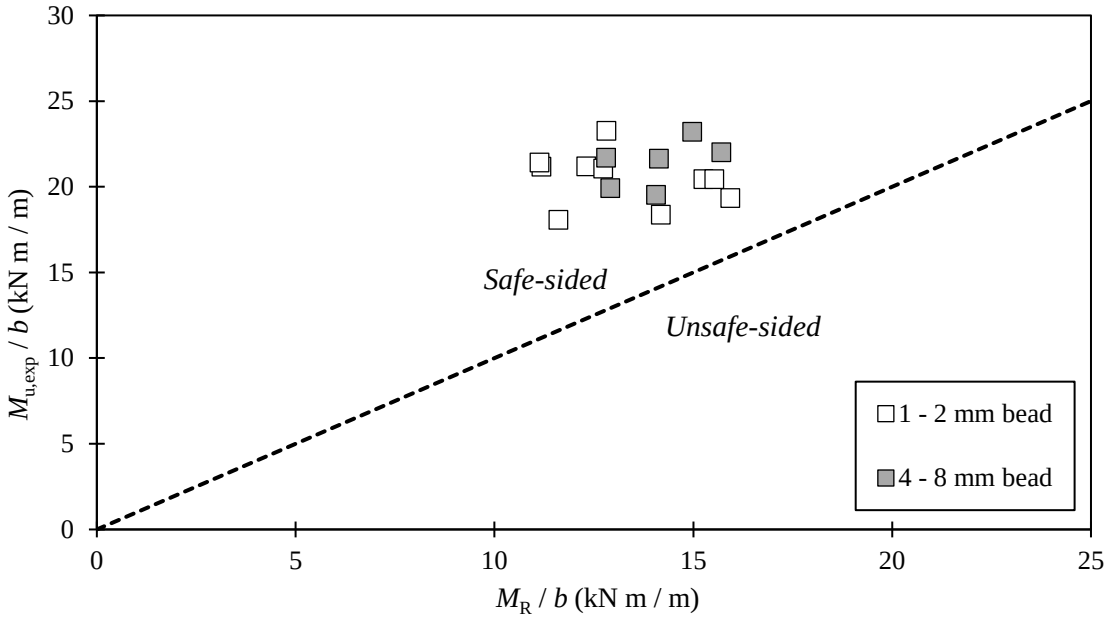

Figure 22: Comparison of experimental and theoretical moments of resistance.

Table 1: Compressive strengths of glass bead core specimens.

Specimen	h (mm)	Bead diameter (mm)	$\sigma_{c,c}$ (N/mm^2)
C01-4-L	130	4 - 8	2.29
C02-1-L	130	1 - 2	2.20
C03-1-S	50	1 - 2	2.08

Table 2: Properties of recycled glass bead composite panels tested in bending.

Specimen ID	Nominal glass bead diameters (mm)	Nominal dimensions (mm) $L_{nom} \times b \times h$	Tested span (mm) L
P01-4-S	4 – 8	1800 × 150 × 152	1650
P02-4-S	4 – 8	1800 × 150 × 152	1650
P03-4-S	4 – 8	1800 × 150 × 152	1650
P04-1-S	1 – 2	1800 × 150 × 152	1650
P05-4-L	4 – 8	2400 × 150 × 152	2250
P06-4-L	4 – 8	2400 × 150 × 152	2250
P07-1-S	1 – 2	1800 × 150 × 152	1650
P08-1-S	1 – 2	1800 × 150 × 152	1650
P09-1-S	1 – 2	1800 × 150 × 152	1650
P10-1-S	1 – 2	1800 × 150 × 152	1650
P11-1-L	1 – 2	2400 × 150 × 152	2250
P12-1-L	1 – 2	2400 × 150 × 152	2250
P13-1-L	1 – 2	2400 × 150 × 152	2250
P14-1-L	1 – 2	2400 × 150 × 152	2250
P15-1-P	1 – 2	2400 × 450 × 152	2250
P16-4-P	4 – 8	2400 × 450 × 152	2250

Table 3: Mechanical properties of recycled glass bead cores.

Specimen	$E_{c,el}$ (N/mm^2)	$\varepsilon_{c,el}$	$\sigma_{c,el}$ (N/mm^2)	$\varepsilon_{c,u}$	$\sigma_{c,u}$ (N/mm^2)	$\varepsilon_{c,u}$ / $\varepsilon_{c,el}$
P01-4-S	939	0.097%	0.88	0.356%	1.32	3.67
P02-4-S	881	0.129%	1.02	0.312%	1.23	2.41
P03-4-S	800	0.153%	1.10	0.277%	1.15	1.82
P04-1-S	997	0.142%	1.35	0.162%	1.39	1.14
P05-4-L	812	0.114%	0.94	0.306%	1.25	2.68
P06-4-L	807	0.052%	0.44	0.291%	1.08	5.56
P07-1-S	1216	0.142%	1.68	0.190%	1.84	1.34
P08-1-S	1159	0.137%	1.56	0.189%	1.80	1.38
P09-1-S	1238	0.138%	1.69	0.229%	1.88	1.65
P10-1-S	1231	0.147%	1.72	0.203%	1.91	1.38
P11-1-L	1059	0.119%	1.20	0.155%	1.28	1.30
P12-1-L	1089	0.129%	1.29	0.151%	1.35	1.18
P13-1-L	1104	0.116%	1.21	0.168%	1.49	1.45
P14-1-L	1131	0.119%	1.34	0.183%	1.52	1.54
P15-1-P	1039	0.158%	1.51	0.176%	1.53	1.12
P16-4-P	984	0.087%	0.87	0.304%	1.41	3.47
1–2 mm bead cores						
- Average	1126	0.135%	1.45	0.181%	1.60	1.35
- COV	0.07	0.10	0.138	0.13	0.15	0.13
4–8 mm bead cores						
- Average	871	0.106%	0.87	0.308%	1.24	3.27
- COV	0.09	0.33	0.26	0.09	0.09	0.40

Table 4: Exemplar span table showing achievable spans (in m) for floor panels with 1–2 mm diameter bead core.

h_c	q_k (kN/m^2)						
(mm)	1.00	1.50	2.00	2.50	3.00	3.50	4.00
50	2.36	2.14	1.97	1.84	1.73	1.64	1.56
75	3.17	2.88	2.65	2.48	2.33	2.21	2.10
100	3.96	3.59	3.31	3.09	2.91	2.75	2.62
125	4.73	4.30	3.96	3.70	3.48	3.29	3.14
150	5.50	5.00	4.61	4.30	4.04	3.83	3.65
175	6.27	5.69	5.25	4.90	4.61	4.36	4.16
200	7.03	6.39	5.89	5.49	5.17	4.90	4.66
225	7.79	7.08	6.53	6.09	5.73	5.43	5.17
250	8.55	7.77	7.16	6.68	6.29	5.95	5.67

Table 5: Exemplar span table showing achievable spans (in m) for floor panels with 4–8 mm diameter bead core.

h_c	q_k (kN/m^2)						
(mm)	1.00	1.50	2.00	2.50	3.00	3.50	4.00
50	2.71	2.46	2.27	2.12	1.99	1.89	1.80
75	3.51	3.19	2.94	2.75	2.58	2.45	2.33
100	4.27	3.88	3.58	3.33	3.14	2.97	2.83
125	5.00	4.54	4.19	3.90	3.67	3.48	3.31
150	5.71	5.19	4.78	4.46	4.20	3.97	3.78
175	6.41	5.82	5.37	5.01	4.71	4.46	4.25
200	7.11	6.45	5.95	5.55	5.22	4.95	4.71
225	7.80	7.08	6.53	6.09	5.73	5.43	5.17
250	8.48	7.70	7.10	6.63	6.23	5.90	5.62